A DT-MRI Validation Framework Using Fluoro Data

Seniha Esen Yuksel

December 14, 2006

Abstract

Most of the previous efforts on enhancing the DT-MRI estimation/smoothing have been based on "what is assumed to be correct"; and there are only very few studies concentrating on the validation of these approaches. This project presents our current efforts and observations for a validation framework. In the scope of this framework, high resolution fluoroscopy slices obtained from the brain stem of a rat are compared with the fibers tract maps obtained from the processing of the Diffusion Tensor Magnetic Resonance images of the same rat. Several steps prior to comparison involve (i) the segmentation of the fibers from the fluoro data and the registration of the fibers for 3D stacking; (ii) processing of the DT-MRI data to obtain the fiber tracts; (iii) 3D registration of the fluoro volume to the DT-MRI data. The details of these steps are further investigated throughout this report.

1 Introduction

Research efforts in the processing of diffusion tensor magnetic resonance imaging (DTMRI) data has increased drastically to understand the anatomical connectivity in the brain. Researchers have been using DT-MRI for segmentation, for fiber tracking, for registration and for visualization; however, very little research has been performed to validate the findings of DT-MRI. As such, in [1], the incorrect fiber trajectories found with DT-MRI were demonstrated on an affected descending motor pathway whose anatomy is well known.

The reason is, DT-MRI fiber tracking algorithms generally assume that the fiber pathways coincide with the orientation of the eigenvector with the highest diffusivity. However, it is well known today that, with such basic approaches, it is very difficult to track the fibers at the fiber crossings. At the crossings, the tensor only gives volume-averaged information about the direction of the fibers as illustrated in Fig. 1; which does not represent the reality. To refrain from such mistakes, the fiber tracts need to be validated using high resolution histological data. However, a gold standard for validation DT-MRI is still lacking; and only a few studies has worked on validation approaches.

Lin *et al.* in [2] superimposed DT-MRI with manganese-enhanced MRI of optic tracts. Although this is an invivo approach that doesn't bring the tissue distortion or destruction problems as in histological methods; long fibers were not enhanced because of the limited transmission of the Mn^{2+} ions. Moreover, the subjective threshold selection for the segmentation of the Mn^{2+}-enhanced pixels introduced varying errors.

Campbell *et al.* [3] applied the flux maximizing flows techique by Vasilevskiy *et al.* [4] to the segmentation of the fibers in histology images. This approach was furthered by Vemuri *et al.* [5] where the segmented fibers were registered to the DT-MRI fiber tracts for validation; but the registration was performed in 2D. Following these studies, Campbell *et al.* [6] validated the performance of their fiber tracking algorithm with a physical phantom constructed from excised rat spinal cords. For fiber tracking high angular resolution diffusion imaging (HARDI) data was used which is known to superiorly handle of the true spatially non-Gaussian diffusion of the medium [7].
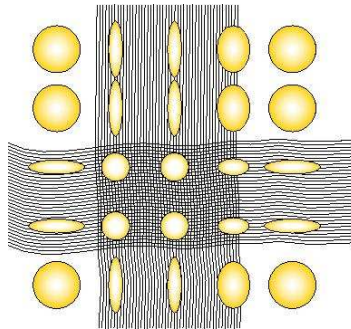
Figure 1: Diffusion Tensor overlying two crossing fibertracts [8].

In this study, we are investigating a framework to validate the fiber tracts obtained from DTI data with the fibers obtained from the fluoroscopy slices. While DTI data gives the connectivity information in the brain stem, the fibers obtained from the fluoro data are used to validate the goodness of the fiber tracts obtained from DTI. In this way, we are hoping to be one step closer to the reality compared to phantom studies.

The sequence of steps below from the scope of our framework, and a figure showing these steps is given in Fig. 2:

1) The fibers in the 2D fluoroscopy slices are first enhanced with a vesselness filter developed by Frangi *et al.* [9].

2) Secondly, the fibers are segmented from the slices using a level set approach developed by Vasilevskiy *et al.* [4].

3) The fluoro slices processed above are not registered to each other as the tissue is distorted and transformed while being cut and placed into the microscope slide. Therefore they cannot be stacked in 3D; but thanks to the landmarks on the left bottom of the histology images, they can be registered and then stacked to form 3D data. Hence, the segmented fibers are treated as point sets and registered simultaneously using the technique described by Wang *et al.* [10]. (At this point, the landmarks on the images are also included in the point set registration). This simultaneous registration cancels the effect of the displacement introduced during the seperate scanning of the histological tissue.

4) The registration parameters obtained from the previous step are applied to the original images to register them (not as point sets, but as images); so that the registered 2D images can be put into a stack in 3D.

5) The 3D stack is again processed with the same vesselness filter this time in 3D.
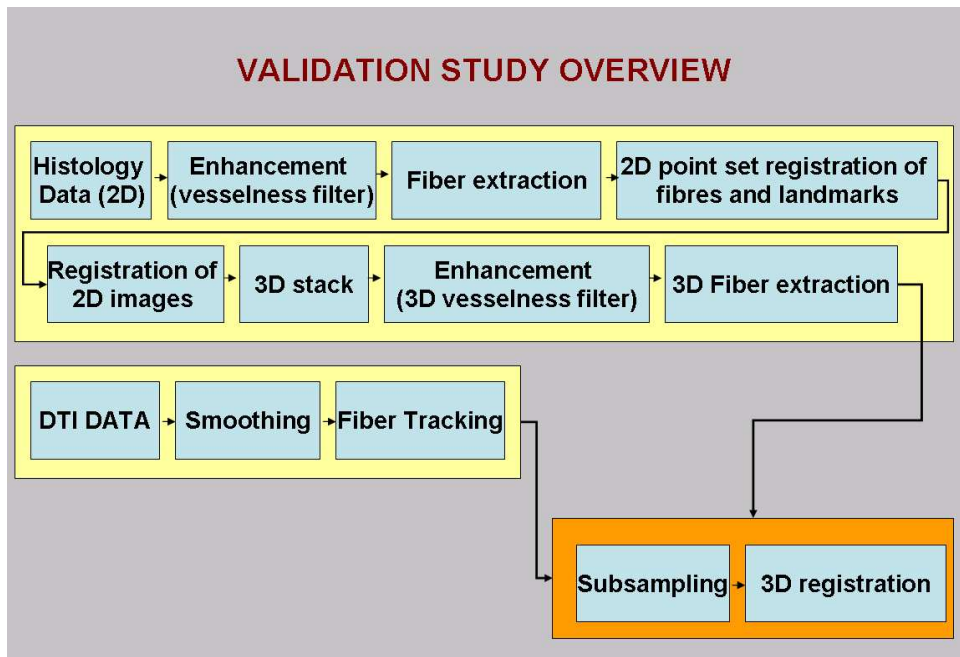
Figure 2: Framework for DT-MRI fiber tracts validation with histology images.

6) The filtered volume is now segmented one more time; but this time in 3D. Hence, the fibers from fluoroscopy images are obtained in 3D.

7) At the same time, DTI is processed to obtain fiber tracts using the algorithm developed by Basser *et al.* [11].

8) The 3D fiber tracts from DTI and the volume of fluoro fibers are regarded as point sets and are registered using the algorithm described in [10]. However; due to high number of points in the registration, and the big difference between the resolutions of these two point sets; the point sets are first randomly sampled. Of the randomly sampled point sets, the affine transformation parameters which give the minimal error is selected.

2 Efforts, Observations and Results:

In this section, we will be detailing each of the eight steps given in the introduction part. We will discuss both the approaches we tried which did not work, and the approaches we found useful to overcome those problems. The math behind the two papers that were implemented is discussed and the results are displayed for all the steps of the framework.

2.1 Data:

The data tested in this project consists of the following:
Fluoroscopy Data 1: 17 images, each of size 1030x1312, slice thickness $40\mu m$
DATA 2: 20 images, first 6 of size 450x357, the rest is of size 450x568.

DT-MRI Data: of size 34x39, 15 slices, slice thickness $200\mu m$.

2.2 Mutual Information Registration – why it didn't work:

At the beginning of our study, we had planned to first register the 2D histological images, and then segment them. For this purpose, we tried mutual information registration; however, two problems are faced: (i) the registration gets biased if we register all the images onto one image; (ii) there is no landmark to evaluate the goodness of the registration. Therefore, we have found that we should first segment the fibers from the histological slices, than register them using a simultaneous point set registration method. The segmentation and point-set registration algorithms will be desribed in the sections below.

2.3 Implementation of Frangi Vesselness Filter:

The Frangi vesselness filter analyses the local behaviours of an image using the Hessian matrix; where the differentiation is defined by a convolution with derivatives of Gaussians [9]:

$$I_x = s^\gamma I(x) * \frac{\partial}{\partial x} G(x, s)$$

where the D-dimensional Gaussian is defined as

$$G(x, s) = \frac{1}{\sqrt{2\pi s^2}^D} e^{-\frac{\|x\|^2}{2s^2}}$$

with γ as the scaling parameter.

With the derivatives so defined, the Hessian matrix can be found as:

$$H = \left[\begin{array}{ccc} I_{xx} & I_{xy} & I_{xz} \\ I_{yx} & I_{yy} & I_{yz} \\ I_{zx} & I_{zy} & I_{zz} \end{array} \right]$$

Let the eigenvalues of H be $|\lambda_1| < |\lambda_2| < |\lambda_3|$. For an ideal tubular structure in a 3D image, the smallest eigenvalue will be close to zero, and the other two eigenvalues will be much bigger and almost equal to each other. Also, these two eigenvalues will be at their maximum at the vessel's centerline. With the eigenvalues sorted as above, the vesselness function in 3D is given as:

$$V_0(s) = \left[\begin{array}{ll} 0 & if \lambda_2 > 0 \ or \ \lambda_3 > 0 \\ (1 - exp(-\frac{R_A^2}{2\alpha^2}))exp(-\frac{R_B^2}{2\beta^2})(1 - exp(-\frac{S^2}{2c^2})) & \end{array} \right]$$

where

$$R_A = \frac{|\lambda_2|}{|\lambda_3|} \quad , \quad R_B = \frac{|\lambda_1|}{\sqrt{|\lambda_2 \lambda_3|}}$$

In 2D, the equations are modified as:

$$V_0(s) = \left[\begin{array}{ll} 0 & if \lambda_2 > 0 \\ exp(-\frac{R_B^2}{2\beta^2})(1 - exp(-\frac{S^2}{2c^2})) & \end{array} \right]$$

4

$$R_B = \frac{|\lambda_1|}{|\lambda_2|}$$

In my implementation, I found $\beta = 5$ and $s = 0.5 to 2$ to be good values. As you increase β, you get more connected lines (but fatter).

2.4 Implementation of Flux Maximizing Flows:

Rather than tracking the movement of a given contour C moving with speed F in its normal direction $\vec{n}$ according to the evolution equation

$$\frac{\partial C}{\partial t} = F\vec{n},$$

we consider the signed distance function ϕ to C and track its motion with the evolution equation

$$\frac{\partial \phi}{\partial t} = F|\nabla\phi|;$$

known as the level sets method [12].

Vasilevskiy *et al.* [4] has proposed a flux maximizing geometric flows approach that has allowed the segmentation of thin blood vessels. The idea here is to evolve a curve to increase the inward flux of a fixed vector field thorough its boundary; where the flow is given by:

$$\frac{\partial C}{\partial t} = div(\vec{V})\vec{N},$$

where $\vec{N}$ is the unit outward normal to each point on the curve C. This flow evolves a curve to a configuration where its normals are aligned with the vector field. In the level sets form, the equation can be written as:

$$\frac{\partial \phi}{\partial t} = div(V)||\nabla\phi||.$$

A major lack in this paper was the fact that the image forces were not given in detail. So, we used a curvature force for smoothness, a constant inflation force to be able to grow, and the flux maximizing flow to attract the level set to zero crossings. Advection forces were not used.

2.5 Point Set Registration in 2D:

After the fiber segmentation of fluoroscopy data, the fibers are treated as point sets. In Fig 7(a), three of the fibers (the crossing points) are displayed with the pointsets obtained from the landmarks in the fluoroscopy data (the circular regions). As it can be seen from the landmarks, the 2D data is not aligned correctly. Hence, these pointsets are registered using the groupwise registration algorithm by Wang *et al.* [13], and nicely aligned without bias as shown in Fig 7(b).

Prior to the registration, the images that don't give significant information on the crossing of the fibers are dropped. Hence six of the images are kept (numbers 13-18), and registered. The registration parameters of these six images are as follows:
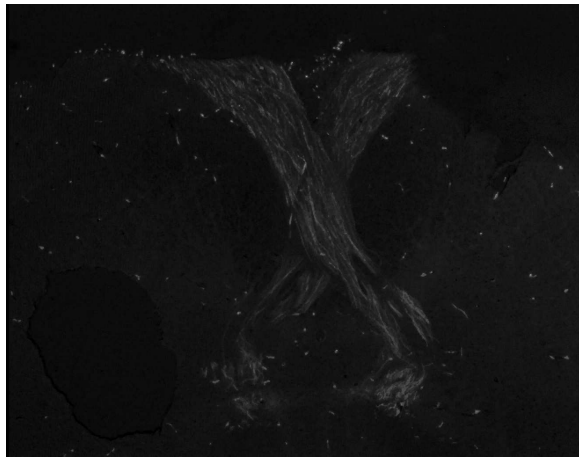
(a)
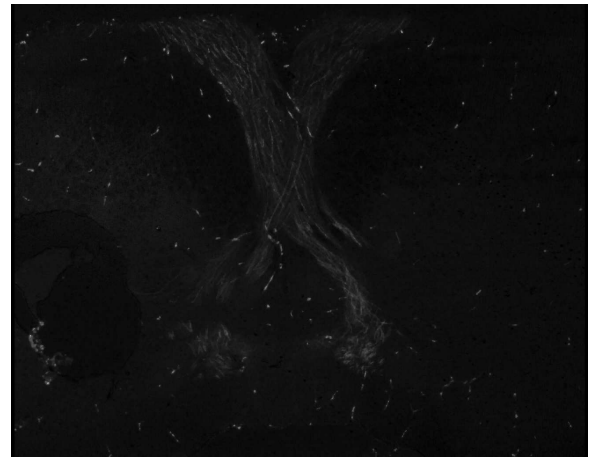
(b)
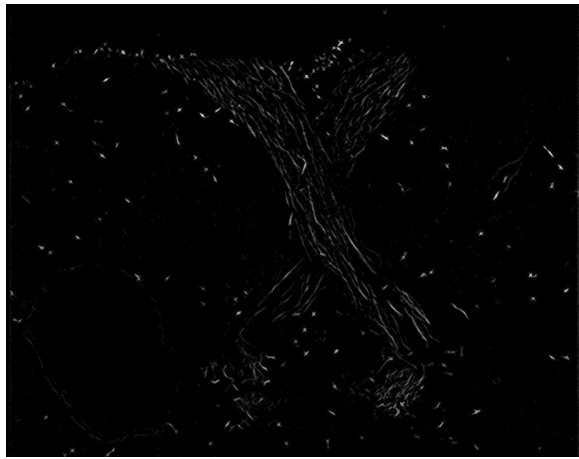
(c)
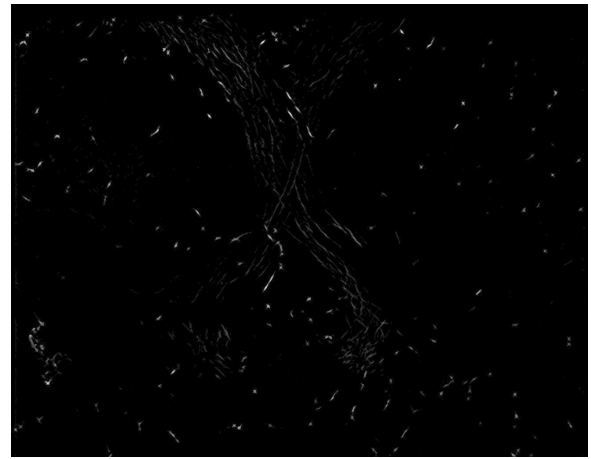
(d)
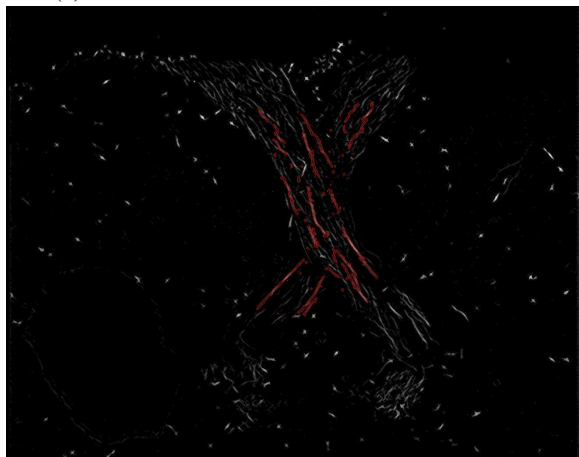
(e)
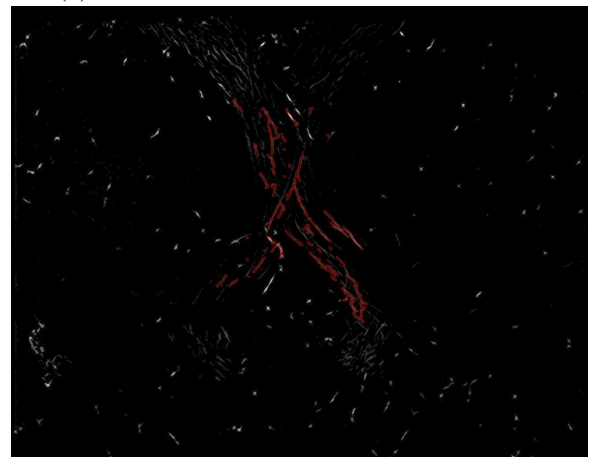
(f)

Figure 3: Results of the vesselness filtering and fiber segmentation of dataset 1, images 5 and 6. The original data is shown in (a) and (b), the vesselness filtered images are shown in (c) and (d) and the fiber segmentation results are shown in (e) and (f); where the final level sets are shown on the fluoroscopy images as red.
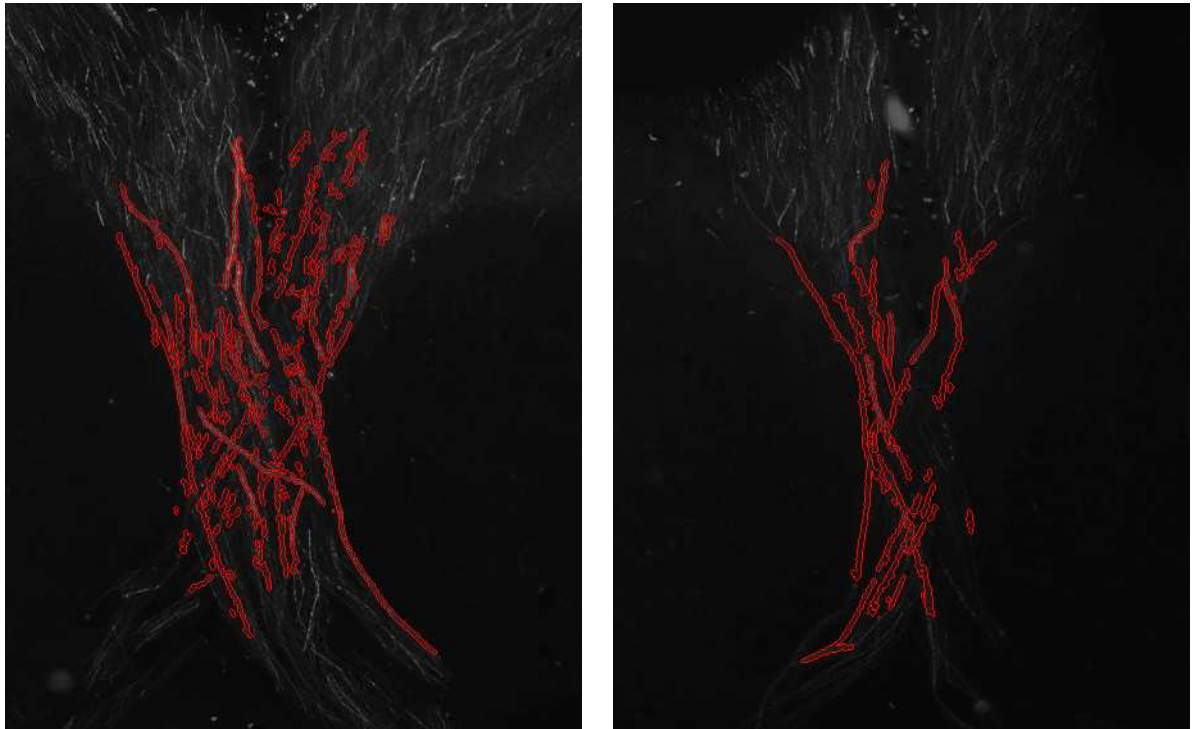
Figure 4: A more detailed image showing the segmented fibers on the second dataset, images 10 and 13. The correspoding level sets are displayed on the fluoroscopy images as red. Among the two datasets we had, this data had better resolution and more distinct fibers; however, it does not have the landmarks necessary for registration –or at least necessary to understand the goodness of registration. Hence, the first dataset is preffered in the rest of this project.
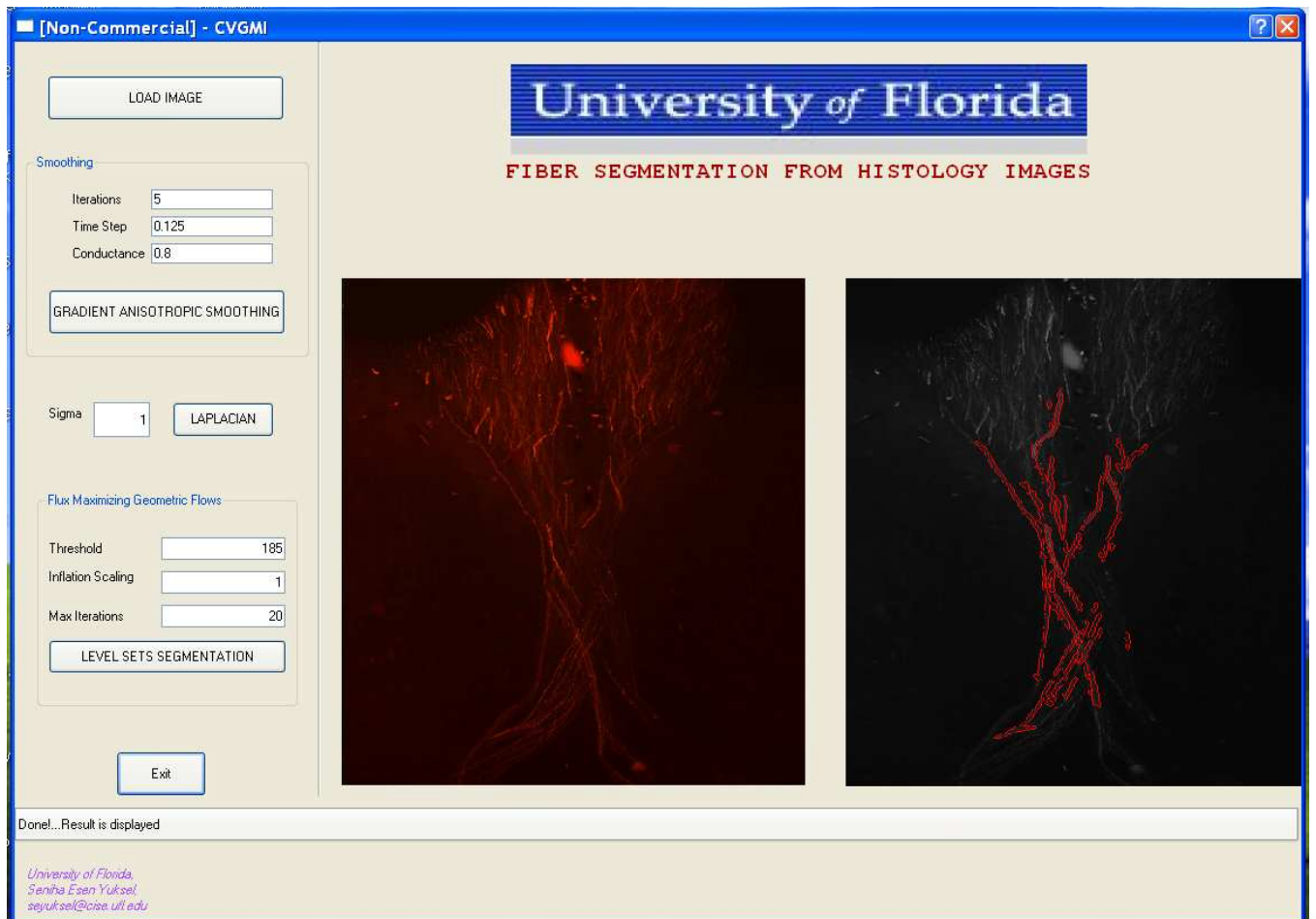
Figure 5: A GUI is implemented which handles the segmentation of the fibers. Also optionally, gradient anisotropic smoothing can be applied to enhance the fibers.
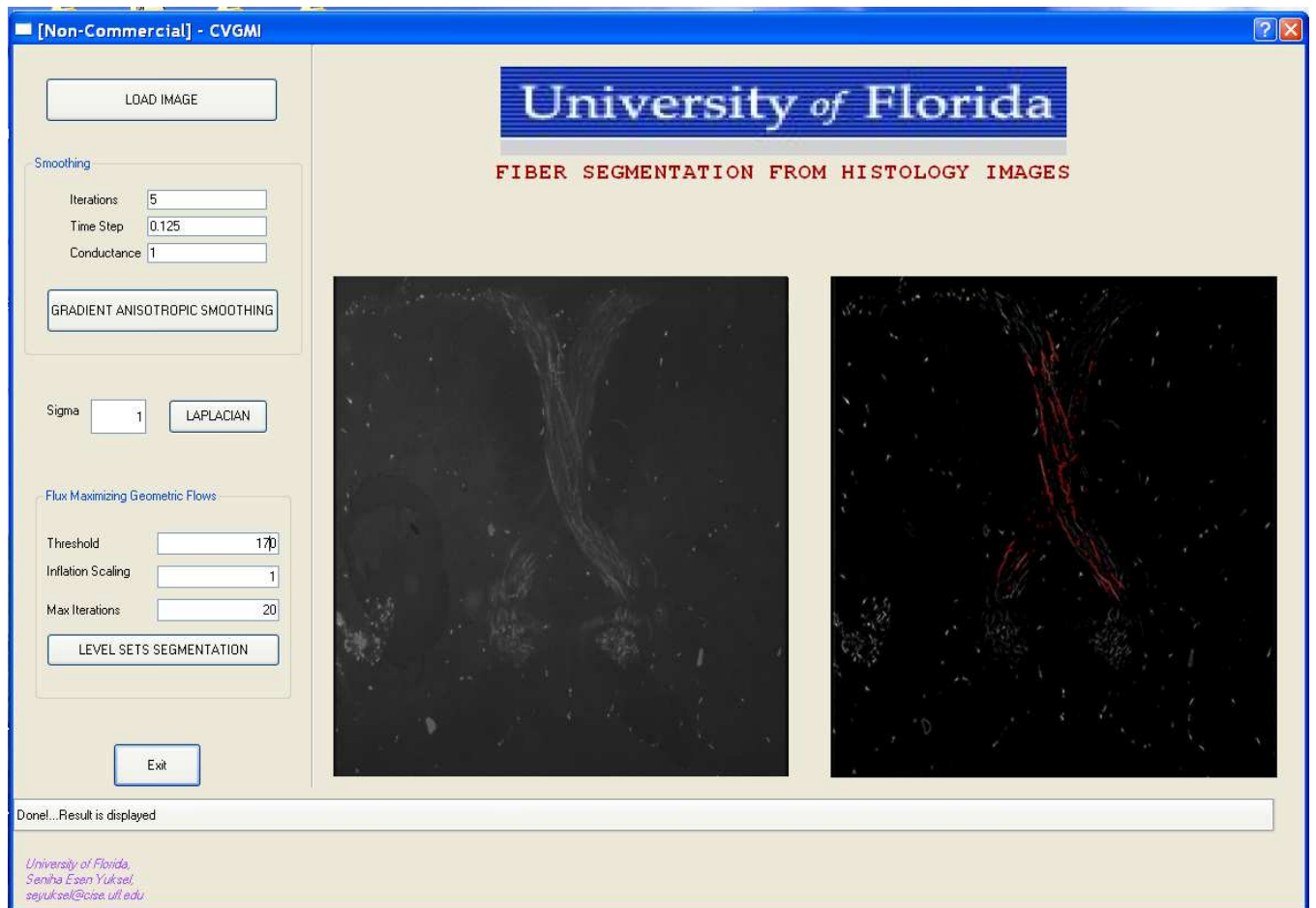
Figure 6: Another screen shot from the GUI which performs the segmentation of the fibers. Also optionally, gradient anisotropic smoothing can be applied to enhance the fibers.
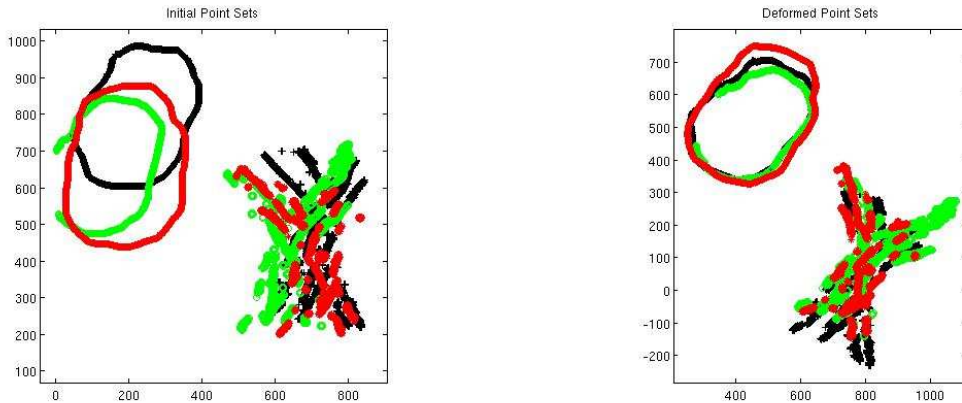
(a)   (b)

Figure 7: The fibers obtained from the fluoroscopy data is displayed on top of each other as point sets. The circular region is the landmarks, and the crossings are the fibers in the brain stem fluoroscopy data. The non-matching landmarks show the initial mis-alignment of the 2D images. The segmented fiber pointsets are combined with the landmark pointsets for registration. The registration results are displayed in (b).

TranslationX, TranslationY, theta:
-46.2374, -137.8723, -0.3655
41.9311, -27.0859, -0.4474
-28.0452, 56.6688, -0.5070
42.3635, 82.3661, -0.4766
14.2967, 51.0205, -0.4748
-24.3037, -25.0920, -0.4670

2.6   Fiber Segmentation in 3D:

With the registration parameters given in the previous section, the original images are transformed as shown in Fig. 8. Hence, the data is now ready for 3D processing. The images are then passes through a 3D vesselness filter and the fibers are segmented once again, but this time in 3D. The segmented fibers are again regarded as pointsets and visualized as in Fig. 9. In this visualization code, the user has the ability to go back and forth between the 2D images while looking at the point set cloud in 3D.

2.7   Point Set Registration in 3D:

At this step of the framework, pointsets are obtained from the DT-MRI data using a fiber tracking algorithm by Basser *et al.* [11]. The expected region of the fiber crossings is shown in Fig. 10(a). The fibers obtained from this region are tracked with a threshold of FA = 0.2; and visualized in Fig. 10(b). When the point sets from the previous section are visualized on top of the point sets obtained from DT-MRI, one can clearly see the need for affine registration in Fig. 11. However, these pointsets are huge, and hard to
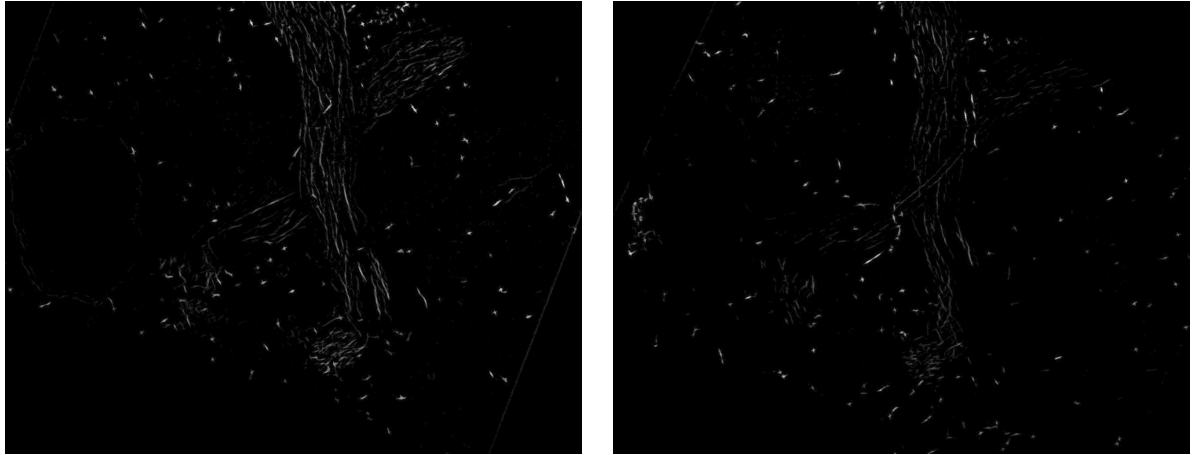
Figure 8: With the transformation parameters obtained from the 2D registration, the original images are transformed.
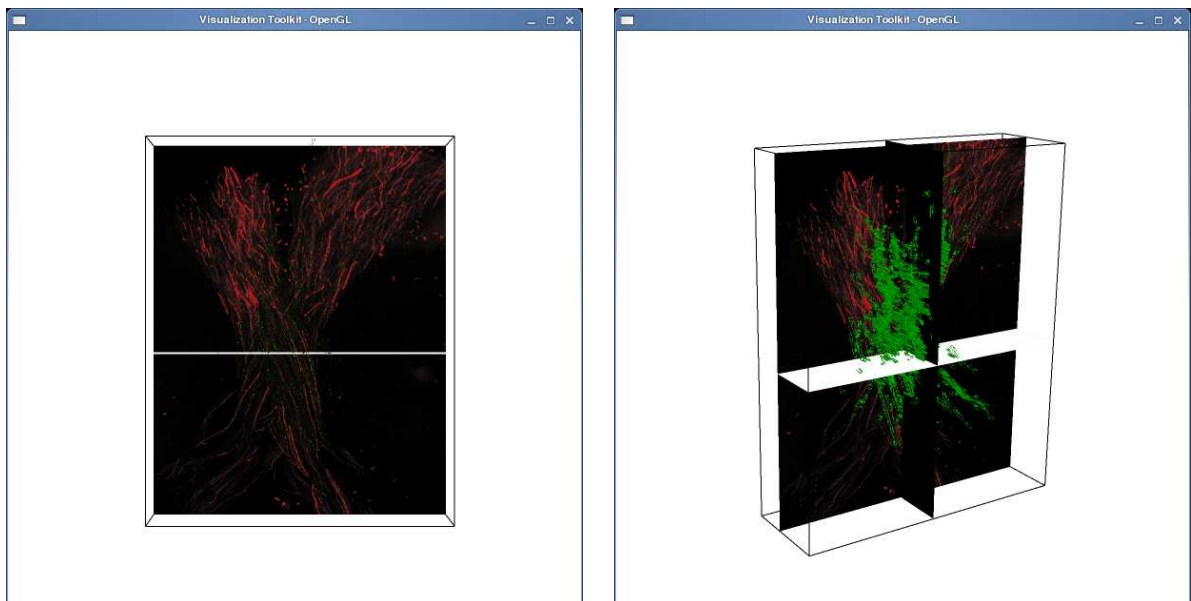
Figure 9: After the registration step, the fibers are segmented again, but this time with the 3D version of the algorithm. The fibers segmented in 3D are visualized in 3D as a point set cloud. The user has the ability to go back and forth between the 2D images, and observe the 3D point set cloud on the 2D images.

align. The fibers from fluoroscopy data can easily get stuck to fibers from DTI with a false transformation. Therefore, the pointsets are randomly decreased to one tenth of their sizes, and then registered. Then the transformation parameters corresponding to the pointset pair with the smallest error are used in registering the original (not subsampled) data. Fig. 10(a) displays the registration of the subsampled pointset pair with the minimal error.

References

[1] Carlo Pierpaoli, Alan S. Barnett, Sinisa Pajevic, Anette Virta, and Peter J. Basser. Validation of dt-mri tractography in the descending motor pathways of human subjects. In *Proc. Intl. Soc. Mag. Reson. Med.*, volume 9, page 501, 2001.

[2] C.P. Lin, W.Y. Tseng, H.C. Cheng, and J.H. Chen. Validation of diffusion tensor magnetic resonance axonal fiber imaging with registered manganese-enhanced optic tracts. *Neuroimage*, 14(5):1035–47, Nov 2001.

[3] J. Campbell, K. Siddiqi, B. Vemuri, and G. Pike. A geometric flow for white matter fibre tract reconstruction. In *In IEEE International Symposium on Biomedical Imaging Conference Proceedings, pages 505–508, July 2002.*, 2002.

[4] A. Vasilevskiy and K. Siddiqi. Flux maximizing geometric flows. *IEEE Trans. Pattern Anal. Mach. Intell.*, 24(12):1565–1578, 2002.

[5] B. C. Vemuri, Y. Chen, M.Rao, Z. Wang, T.McGraw, T.Mareci, S.J.Blackband, and P.Reier. Automatic fiber tractography from dti and its validation. In *IEEE International Symposium on Biomedical Imaging Macro to Nano.*, pages 501–504, 2002.

[6] J.S. Campbell, K. Siddiqi, V.V. Rymar, A.F. Sadikot, and G.B. Pike. Flow-based fiber tracking with diffusion tensor and q-ball data: validation and comparison to principal diffusion direction techniques. *Neuroimage*, 27(4):725–36, Oct 2005.

[7] D.S. Tuch, R.M. Weisskoff, J.W. Belliveau, and V.J. Wedeen. High angular resolution diffusion imaging of the human brain. In *Proceedings of the 7th Annual Meeting of ISMRM*, page 321, 1999.

[8] Raimundo Sierra. Nonrigid registration of diffusion tensor images. Master's thesis, Swiss Federal Institute of Technology, 2001.

[9] A.F. Frangi, W.J. Niessen, K.L. Vincken, and M.A. Viergever. Multiscale vessel enhancement filtering. In MICCAI'98, W.M. Wells, A. Colchester, and S.L. Delp, editors, *Medical Image Computing and Computer-Assisted Intervention. Lecture Notes in Computer Science. Springer Verlag, Berlin, Germany.*, volume 1496, pages 130–137, 1998.

[10] F. Wang, B. Vemuri, A. Rangarajan, I. Schmalfuss, and S. Eisenschenk. Simultaneous nonrigid registration of multiple point sets and atlas construction. In *9th European Conference on Computer Vision*, 2006.

[11] P.J. Basser, S. Pajevic, C. Pierpaoli, J. Duda, and A. Aldroubi. In vivo fiber tractography using dt-mri data. *Magnetic Resonance in Medicine*, 44:625–632, 2000.
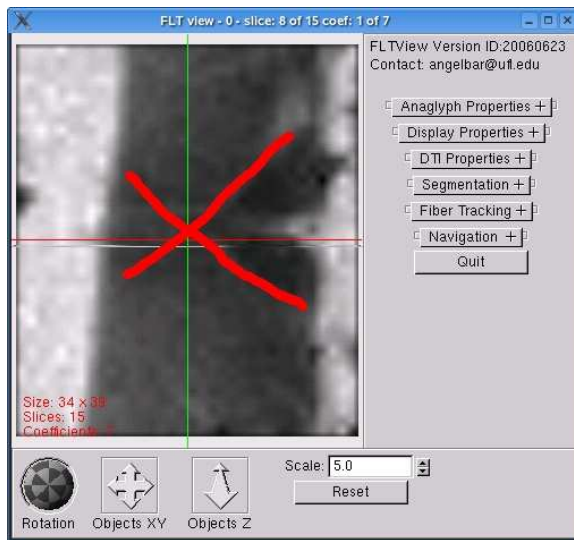
(a)
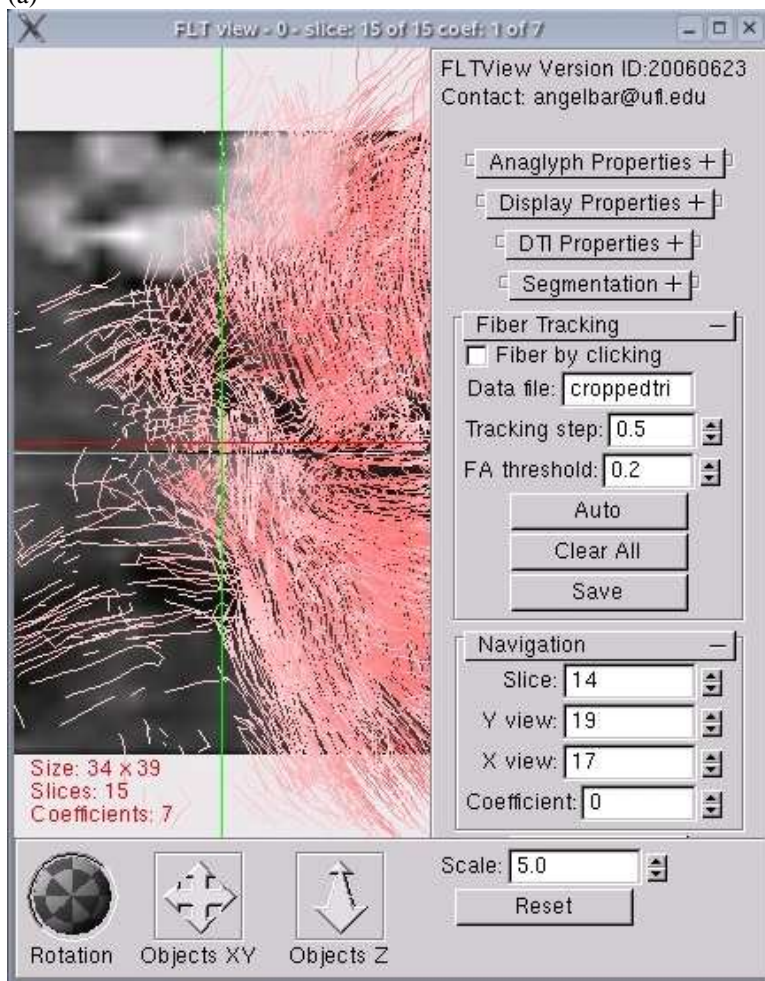
(b)

Figure 10: The red mark on the S0 image of the DTI shows the expected region of the fiber crossings (a). The fibers in this region are tracked and visualized by the FLTView software written by Angelos Barmpoutis [14].
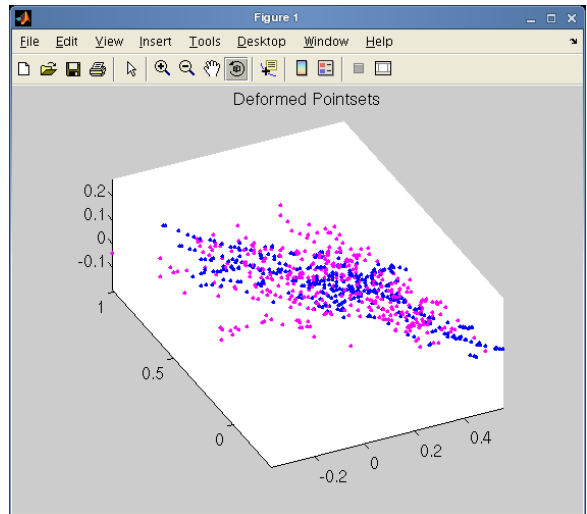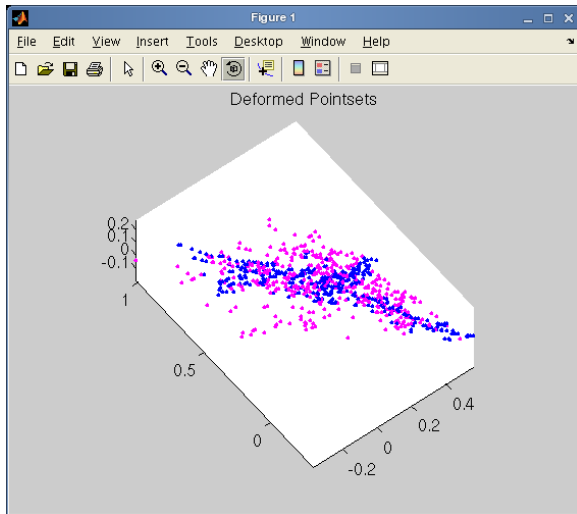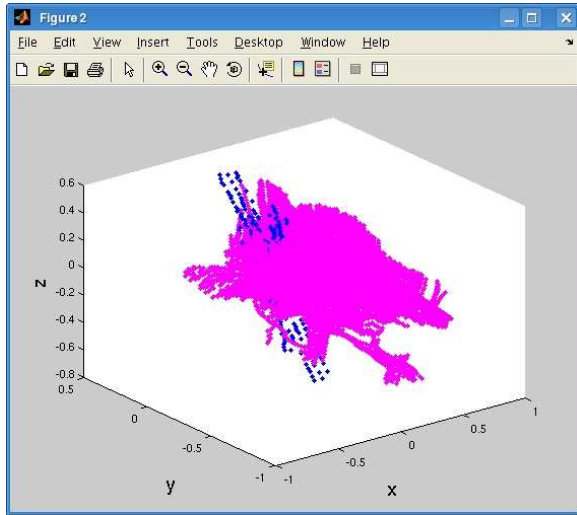
Figure 11: Both the DT-MRI fiber tracts (shown in pink) and the fluoroscopy fibers (shown in blue) are treated as point sets. The initial pointsets in (a) are subsampled, and affine registered with the algorithm by Wang [10] as shown in (b) and (c) in from two different views.
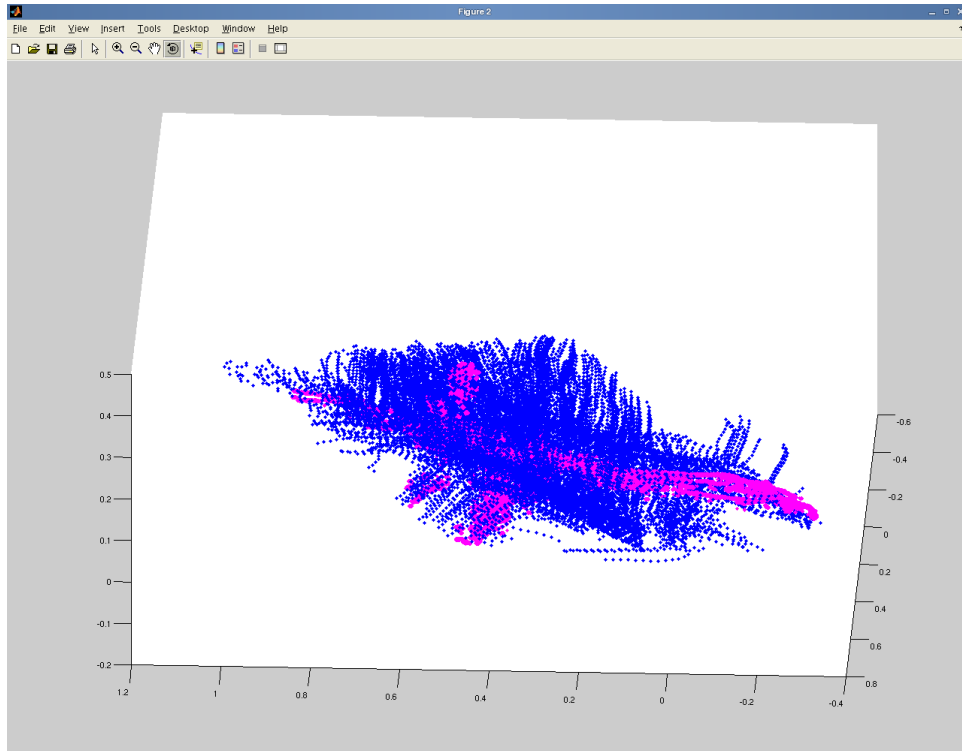
(a)
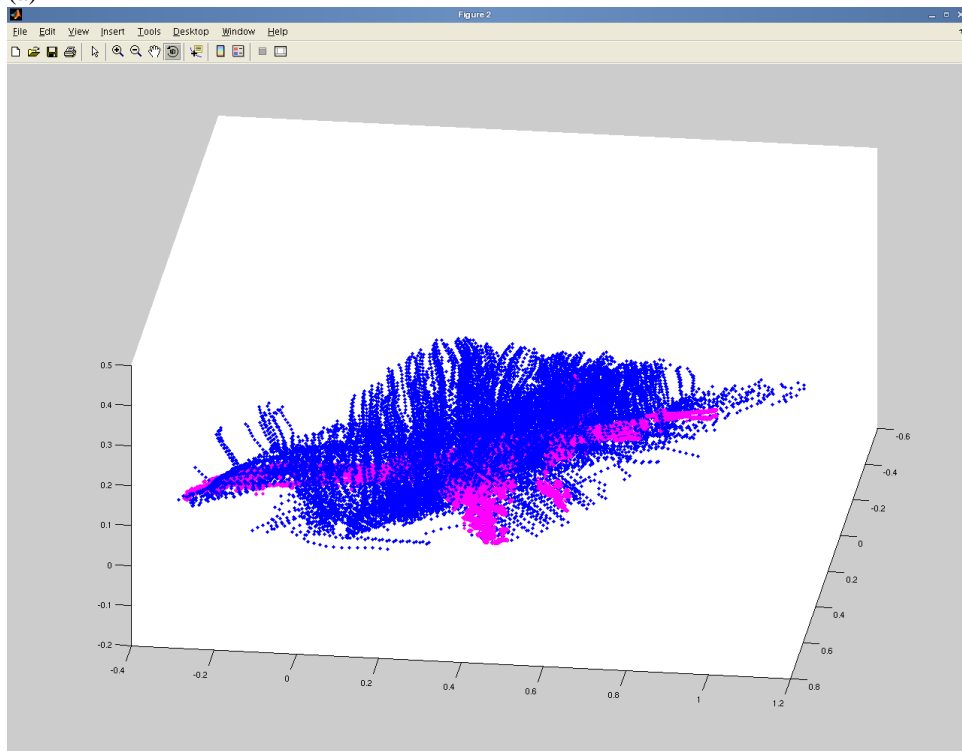
(b)

Figure 12: The final result of registering the fibers – from DT-MRI (in blue) and from fluoro (in pink).

[12] R. Malladi, J.A. Sethian, and B.C. Vemuri. Shape modeling with front propagation: A level set approach. *IEEE Trans. Pattern Anal. Mach. Intell.*, 17(2):158–175, 1995.

[13] Fei Wang, Baba C. Vemuri, and Anand Rangarajan. Groupwise point pattern registration using a novel cdf-based jensen-shannon divergence. In *CVPR (1)*, pages 1283–1288, 2006.

[14] Angelos Barmpoutis. Fltview diffusion tensor mri visualization tool and flt format file viewer, 2006.